Eur. Phys. J. Plus (2019) **134**: 555
DOI 10.1140/epjp/i2019-12912-7

THE EUROPEAN PHYSICAL JOURNAL PLUS

Regular Article

A comparison for the non-classical plate model based on axial buckling of single-layered graphene sheets

A.M. Fattahi[1,a], B. Safaei[2], and N.A. Ahmed[1]

[1] Department of Mechanical Engineering Science, Faculty of Engineering and Built Environment, University of Johannesburg, 2006, Johannesburg, South Africa
[2] Department of Mechanical Engineering, Tsinghua University, Beijing 100084, China

Received: 5 February 2019 / Revised: 15 July 2019
Published online: 8 November 2019

Abstract. In this study, the size effect on the axial buckling behavior of single-layered graphene sheets embedded in elastic foundation is studied. Eringen's non-local elasticity equations are incorporated into first-order shear deformation, higher-order shear deformation, and classical plate theories. Values of Winkler and Pasternak moduli parameters, side lengths of square SLGSs, non-local parameter and mode numbers are obtained from different non-local plate theories. It is shown that the axial buckling behavior is strongly dependent on non-local parameters and moduli which are different for different numbers and side lengths. Furthermore, we find that non-locality is more influential in first-order shear deformation than other non-local plate theories, especially in certain ranges of non-local parameters. Sensitivity indices are determined based on the Sobol method in their corresponding physical ranges.

1 Introduction

The behaviors of nanostructures were predicted under different loading conditions using theoretical methods. Kitipornchai *et al.* [1] used a continuum model based on classical plate theory to investigate the vibration of multi layered graphene sheets under simply supported boundary conditions. The vibration responses of MLSGs embedded in elastic matrices were investigated using a continuum model by Liew *et al.* [2]. The nanoscale vibration of MLSGs embedded in elastic foundation was studied by Behfar *et al.* [3]. They considered each MLSGs layer to be an orthotropic plate with different elastic modulus along two perpendicular directions. Free vibration of shells and plate-shell assembly in the background introduction. These kinds of plates and shells are commonly used in engineering. Huang *et al.* [4–6] evaluated the effects of damping and vibration on sandwich structures with elastic-viscoelastic-elastic cores using finite element method.

Peddieson *et al.* [7] used non-local elasticity was to evaluate size effects on micro- and nano-scale structures. They studied the bending of micro- and nano-beams using non-local elasticity theory and found that size had significant effect on nano-structures. Due to its efficiency and simplicity in analyzing the behaviors of different nanostructures, the non-local continuum model has attracted the interest of researchers [8–19]. Fattahi *et al.* [20] investigated the postbuckling behavior of FG-CNTs reinforced nanoshells under hydrostatic pressures. Some researchers [21,22] studied three-dimensional and thermal vibration of FGM beams by using a higher-order shear deformation theory.

Like many other nano-scaled compounds, nanostructures were embedded in elastic surroundings giving polymer nanostructures. Generally, the Winkler foundation model is used to simulate these elastic foundation [23]. However, this model is not able to consider medium continuity. Pasternak foundation model can model elastic foundation more practically [24,25] because it can take into account both transverse normal pressure and shear stress by introducing two modulus parameters corresponding to each factor. Liew *et al.* [26] employed the Pasternak foundation model. Pradhan *et al.* [27] used the nonlocal elasticity theory to investigate the buckling behavior of single-layered graphene sheet (SLGS) embedded in an elastic medium. They modified the classical plate model for SLGS with nonlocal elasticity. They used the differential quadrature method for equation. Furthermore, the nonlinear free vibration of embedded nanobeams was investigated Azizi *et al.* [28]. The mesh-free method was used to study free vibration, thermoelastic and resonance characteristics of finite length functionally graded nanocomposite cylinders [29,30]. Free vibration [31–34],

[a] e-mail: afattahi@uj.ac.za (corresponding author)

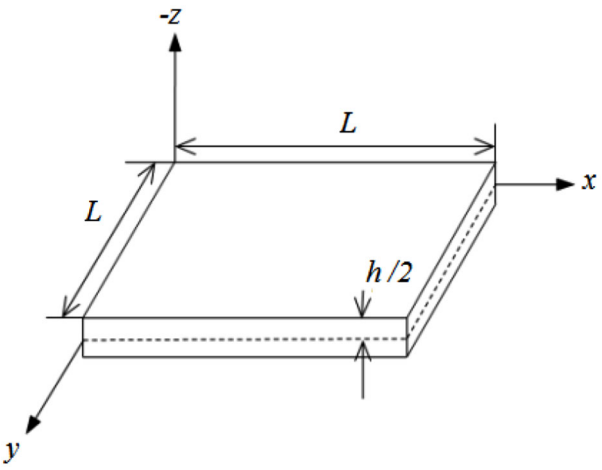

Fig. 1. Schematic diagram of a nanoplate.

stress distributions [35], thermoelastic vibration and dynamic [36–38] behaviors of sandwich plates with aggregated CNTs reinforced nancomposite face sheets on elastic foundations were studied by using different plate and shell theories.

To evaluate the buckling properties of single graphene sheet, Bouadi *et al.* [39] introduced a novel non-local higher-order shear deformation theory. Ebrahimi *et al.* [40] suggested that surface effect, thermal loading type, temperature change, boundary conditions, plate thickness, and non-local parameter significantly influenced flexoelectric nanoplates buckling loads. Daouadji *et al.* [41] compared numerical results with quasi-3-dimensional solutions, 3D exact solutions, and other higher-order shear deformation theories. Malikan *et al.* [42,43] analyses buckling behavior of plate and nanoplate by using couple stress theory. Safaei *et al.* [44] studied critical axial buckling strain of CNTs with different chiral angles. Fattahi *et al.* [45] revealed that the stiffness of nanocomposite beams increased with higher volume fractions of CNTs, especially long SWCNT. Many researchers studied non-linear static stability, bending, forced vibration of beams, plates, shells, graphene and nanosheets [46–58] by using unified solution, nonlocal and refined plate theory and finite element method. Safaei *et al.* [59] investigated mechanical and thermal benefits of porosity in sandwich structures by using mesh-free methods.

Here, we have investigated size effect on the axial buckling of embedded SLGSs by incorporating Eringen's non-local elasticity equations [60] into different plate theories and obtained equations for critical axial buckling loads for each non-local plate theory. Furthermore, different numerical results have been provided to validate the effects of length, non-local parameter and mode number in Winkler and Pasternak foundation models separately. Finally, sensitivity indices have been determined based on Sobol method in their corresponding physical ranges [61].

Prediction of the elastic properties of graphene-reinforced sheets and graphene plates is among the applications of this research. The innovative aspect of this research is employing Eringen's non-local theory in three plate theories. Furthermore, application of Fourier's method to solve equations and comparing the three modified theories for nanoscale are other innovations of this study.

2 Overview of different plate theories

2.1 Introduction

As is shown in fig. 1, a uniform square nanoplate with dimensions L and h (side length and thickness) was considered. A coordinate system (x, y, z) was considered at one corner of nanoplate midplane in such a way that the x-, y- and z-axes were along the length, width and depth directions, respectively.

Displacement components (u, v, w) in their corresponding axes (x, y, z) were stated as [62,63]

$$\begin{aligned} u(x,y,z,t) &= u_0(x,y,t) - z\frac{\partial w}{\partial x} + \psi(z)\left(\frac{\partial w}{\partial x} + \varphi_x\right), \\ v(x,y,z,t) &= v_0(x,y,t) - z\frac{\partial w}{\partial y} + \psi(z)\left(\frac{\partial w}{\partial y} + \varphi_y\right), \\ w(x,y,z,t) &= w_0(x,y,t), \end{aligned} \tag{1}$$

where u_0, v_0 and w_0 are mid-plate displacement components at $z = 0$, $\psi(z)$ is a shape function, and φ_x, φ_y are rotational displacements around y- and x-axis, respectively. For CLPT, $\psi(Z) = 0$, FSDT, $\psi(z) = z$ and HSDT, $\psi(z) = z(1 - \frac{4z^2}{3h^2})$ [63].

2.2 Classical plate theory (CLPT)

Based on eq. (1), strain-displacement equations for CLPT are given as [13]

$$\varepsilon_{xx} = \frac{\partial u}{\partial x} = -z\frac{\partial^2 w}{\partial x^2}\,, \tag{2a}$$

$$\varepsilon_{yy} = \frac{\partial v}{\partial y} = -z\frac{\partial^2 w}{\partial y^2}\,, \tag{2b}$$

$$\gamma_{xy} = \frac{\partial u}{\partial y} + \frac{\partial v}{\partial x} = -2z\frac{\partial^2 w}{\partial x \partial y}\,, \tag{2c}$$

$$\gamma_{xz} = \gamma_{yz} = 0. \tag{2d}$$

Based on the virtual displacement principle, the following equation can be achieved for CLPT:

$$\frac{\partial^2 M_{xx}}{\partial x^2} + \frac{\partial^2 M_{yy}}{\partial y^2} + 2\frac{\partial^2 M_{xy}}{\partial x \partial y} - P\left(\frac{\partial^2 w}{\partial x^2} + \frac{\partial^2 w}{\partial y^2}\right) = 0, \tag{3}$$

where M is the torque vector and P is the critical axial buckling load as

$$M = \{M_{xx}, M_{yy}, M_{xy}\}^T = \int_{-h/2}^{h/2} \{\sigma_{xx}, \sigma_{yy}, \sigma_{xy}\}^T z \cdot \mathrm{d}z, \tag{4a}$$

$$M_{xx} = -D\left(\frac{\partial^2 w}{\partial x^2} + \upsilon\frac{\partial^2 w}{\partial y^2}\right),$$

$$M_{yy} = -D\left(\frac{\partial^2 w}{\partial y^2} + \upsilon\frac{\partial^2 w}{\partial x^2}\right), \tag{4b}$$

$$M_{xy} = -D(1-\upsilon)\left(\frac{\partial^2 w}{\partial x \partial y}\right), \tag{4c}$$

$$D = \frac{Eh^3}{12(1-\upsilon^2)}\,. \tag{4d}$$

The governing equation (3) was written in terms of displacements as follows:

$$-\frac{Eh^3}{12(1-\nu^2)}\left(\frac{\partial^4 w}{\partial x^4} + 2\nu\frac{\partial^4 w}{\partial x^2 \partial y^2} + \frac{\partial^4 w}{\partial y^4}\right) - \frac{Eh^3}{6(1+\nu)}\frac{\partial^4 w}{\partial x^2 \partial y^2} - P\left(\frac{\partial^2 w}{\partial x^2} + \frac{\partial^2 w}{\partial y^2}\right) = 0. \tag{5}$$

2.3 First-order shear deformation theory (FSDT)

FSDT considers the effects of shear deformation and rotational inertia. Therefore, the straight lines vertical to the mid-plane of the plate disappear. However, linear distribution along plate thickness was assumed for transverse shear stress. The following strain-displacement equations could be expressed based on eq. (1) [13]

$$\varepsilon_{xx} = \frac{\partial u_1}{\partial x} = z\frac{\partial \varphi_x}{\partial x}\,, \tag{6a}$$

$$\varepsilon_{yy} = \frac{\partial u_2}{\partial y} = z\frac{\partial \varphi_y}{\partial y}\,, \tag{6b}$$

$$\gamma_{xy} = \frac{\partial u_1}{\partial y} + \frac{\partial u_2}{\partial x} = z\left(\frac{\partial \varphi_x}{\partial y} + \frac{\partial \varphi_y}{\partial x}\right), \tag{6c}$$

$$\gamma_{xz} = \frac{\partial u_1}{\partial z} + \frac{\partial u_3}{\partial x} = \frac{\partial w}{\partial x} + \varphi_x, \tag{6d}$$

$$\gamma_{yz} = \frac{\partial u_2}{\partial z} + \frac{\partial u_3}{\partial y} = \frac{\partial w}{\partial y} + \varphi_y. \tag{6e}$$

According to the virtual displacement principle, the following equations are obtained for FSDT:

$$\frac{\partial Q_{xx}}{\partial x}+\frac{\partial Q_{yy}}{\partial y}-P\left(\frac{\partial^2 w}{\partial x^2}+\frac{\partial^2 w}{\partial y^2}\right)=0, \tag{7a}$$

$$\frac{\partial M_{xx}}{\partial x}+\frac{\partial M_{xy}}{\partial y}-Q_{xx}=0, \tag{7b}$$

$$\frac{\partial M_{yy}}{\partial y}+\frac{\partial M_{xy}}{\partial x}-Q_{yy}=0, \tag{7c}$$

$$\{Q_x,Q_y\}^T=\kappa\int_{-h/2}^{h/2}\{\sigma_{yz},\sigma_{xz}\}^T\mathrm{d}z, \tag{7d}$$

where Q is the shear force per unit length and κ is the shear correction coefficient. The governing equation (6) was written in terms of displacements as

$$\kappa Gh\left(\frac{\partial\varphi_x}{\partial x}+\frac{\partial\varphi_y}{\partial y}+\frac{\partial^2 w}{\partial x^2}+\frac{\partial^2 w}{\partial y^2}\right)-P\left(\frac{\partial^2 w}{\partial x^2}+\frac{\partial^2 w}{\partial y^2}\right)=0, \tag{8a}$$

$$\frac{Eh^3}{12(1-\nu^2)}\left(\frac{\partial^2\varphi_x}{\partial x^2}+\nu\frac{\partial^2\varphi_y}{\partial x\partial y}\right)+\frac{Eh^3}{24(1+\nu)}\left(\frac{\partial^2\varphi_y}{\partial x\partial y}+\frac{\partial^2\varphi_x}{\partial y^2}\right)-\kappa Gh\left(\varphi_x+\frac{\partial w}{\partial x}\right)=0, \tag{8b}$$

$$\frac{Eh^3}{12(1-\nu^2)}\left(\frac{\partial^2\varphi_y}{\partial y^2}+\nu\frac{\partial^2\varphi_x}{\partial x\partial y}\right)+\frac{Eh^3}{24(1+\nu)}\left(\frac{\partial^2\varphi_y}{\partial x^2}+\frac{\partial^2\varphi_x}{\partial x\partial y}\right)-\kappa Gh\left(\varphi_y+\frac{\partial w}{\partial y}\right)=0. \tag{8c}$$

2.4 Higher-order shear deformation theory (HSDT)

In HSDT, the distribution of transverse shear stress along the thickness of the plate was parabolic with no shear correction factor to satisfy transverse shear stress conditions on the lower and upper layers of plate cross-section. Strain-displacement equations for HSDT are obtained, according to eq. (1), as [13]

$$\varepsilon_{xx}=\frac{\partial u_1}{\partial x}=z\frac{\partial\varphi_x}{\partial x}-\frac{4z^3}{3h^2}\left(\frac{\partial\varphi_x}{\partial x}+\frac{\partial^2 w}{\partial x^2}\right), \tag{9a}$$

$$\varepsilon_{yy}=\frac{\partial u_2}{\partial y}=z\frac{\partial\varphi_y}{\partial y}-\frac{4z^3}{3h^2}\left(\frac{\partial\varphi_y}{\partial y}+\frac{\partial^2 w}{\partial y^2}\right), \tag{9b}$$

$$\gamma_{xy}=\frac{\partial u_1}{\partial y}+\frac{\partial u_2}{\partial x}=z\left(\frac{\partial\varphi_x}{\partial y}+\frac{\partial\varphi_y}{\partial x}\right)-\frac{4z^3}{3h^2}\left(\frac{\partial\varphi_x}{\partial y}+\frac{\partial\varphi_y}{\partial x}+2\frac{\partial^2 w}{\partial x\partial y}\right), \tag{9c}$$

$$\gamma_{xz}=\left(1-\frac{4z^2}{h^2}\right)\left(\frac{\partial w}{\partial x}+\varphi_x\right), \tag{9d}$$

$$\gamma_{yz}=\left(1-\frac{4z^2}{h^2}\right)\left(\frac{\partial w}{\partial y}+\varphi_y\right). \tag{9e}$$

Based on the virtual displacement principle, the following equations can be given for HSDT:

$$\frac{\partial Q_{xx}}{\partial x}+\frac{\partial Q_{yy}}{\partial y}-\frac{4}{h^2}\left(\frac{\partial S_{xx}}{\partial x}+\frac{\partial S_{yy}}{\partial y}\right)+\frac{4}{3h^2}\left(\frac{\partial^2 R_{xx}}{\partial x^2}+\frac{\partial^2 R_{yy}}{\partial y^2}+2\frac{\partial^2 R}{\partial x\partial y}\right)-P\left(\frac{\partial^2 W}{\partial x^2}+\frac{\partial^2 W}{\partial y^2}\right)=0, \tag{10a}$$

$$\frac{\partial M_{xx}}{\partial x}+\frac{\partial M_{xy}}{\partial y}-\frac{4}{3h^2}\left(\frac{\partial R_{xx}}{\partial x}+\frac{\partial R_{xy}}{\partial y}\right)-Q_{xx}+\frac{4}{h^2}S_{xx}=0, \tag{10b}$$

$$\frac{\partial M_{yy}}{\partial y}+\frac{\partial M_{xy}}{\partial x}-\frac{4}{3h^2}\left(\frac{\partial R_{yy}}{\partial y}+\frac{\partial R_{xy}}{\partial x}\right)-Q_{yy}+\frac{4}{h^2}S_{yy}=0, \tag{10c}$$

where

$$R=\{R_{xx},R_{yy},R_{xy}\}^T=\int_{-h/2}^{h/2}Z^3\{\sigma_{xx},\sigma_{yy},\sigma_{xy}\}^T\mathrm{d}z$$

and

$$S=\{S_{xx},S_{yy}\}^T=\int_{-h/2}^{h/2}Z^2\{\sigma_{xz},\sigma_{yz}\}^T\mathrm{d}z.$$

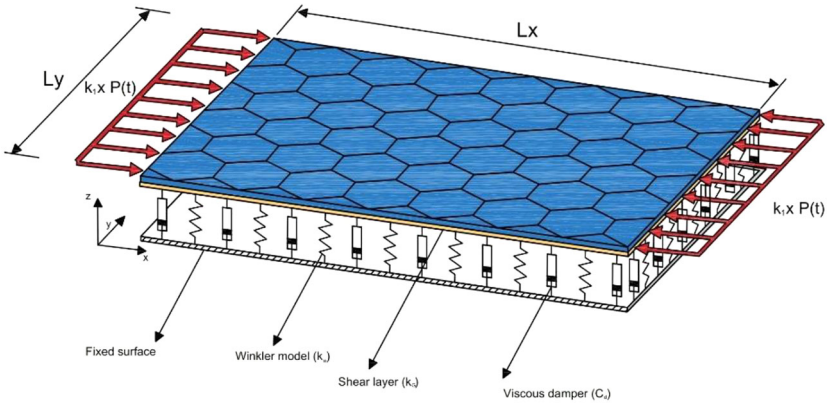

Fig. 2. Schematic diagram of the rectangular plate under axial loads embedded in elastic foundation modeled by the Pasternak foundation model.

The governing equation (10) is expressed in terms of displacements as

$$\frac{8Gh}{15}\left(\frac{\partial\varphi_x}{\partial x}+\frac{\partial\varphi_y}{\partial y}+\frac{\partial^2 w}{\partial x^2}+\frac{\partial^2 w}{\partial y^2}\right)+\frac{4Eh^3}{315(1-\nu^2)}\left[\frac{\partial^3\varphi_x}{\partial x^3}+\frac{\partial^3\varphi_y}{\partial y^3}+\nu\left(\frac{\partial^3\varphi_x}{\partial x\partial y^2}+\frac{\partial^3\varphi_y}{\partial x^2\partial y}\right)\right]$$
$$-\frac{4Eh^3}{252(1-\nu^2)}\left(\frac{\partial^4 w}{\partial x^4}+\frac{\partial^4 w}{\partial y^4}+2\nu\frac{\partial^4 w}{\partial x^2\partial y^2}\right)+\frac{4Eh^3}{315(1+\nu)}\left(\frac{\partial^3\varphi_y}{\partial x^2\partial y}+\frac{\partial^3\varphi_x}{\partial x\partial y^2}\right)-P\left(\frac{\partial^2 w}{\partial x^2}+\frac{\partial^2 W}{\partial y^2}\right)=0, \tag{11a}$$

$$\frac{17Eh^3}{315(1-\nu^2)}\left(\frac{\partial^2\varphi_x}{\partial x^2}+\nu\frac{\partial^2\varphi_y}{\partial x\partial y}\right)-\frac{4Eh^3}{315(1-\nu^2)}\left(\frac{\partial^3 w}{\partial x^3}+\nu\frac{\partial^3 w}{\partial x\partial y^2}\right)$$
$$+\frac{17Eh^3}{630(1+\nu)}\left(\frac{\partial^2\varphi_y}{\partial x\partial y}+\frac{\partial^2\varphi_x}{\partial y^2}\right)-\frac{4Eh^3}{315(1+\nu)}\frac{\partial^3 w}{\partial x\partial y^2}-\frac{8Gh}{15}\left(\varphi_x+\frac{\partial w}{\partial x}\right)=0, \tag{11b}$$

$$\frac{17Eh^3}{315(1-\nu^2)}\left(\frac{\partial^2\varphi_y}{\partial y^2}+\nu\frac{\partial^2\varphi_x}{\partial x\partial y}\right)-\frac{4Eh^3}{315(1-\nu^2)}\left(\frac{\partial^3 w}{\partial y^3}+\nu\frac{\partial^3 w}{\partial y\partial x^2}\right)$$
$$+\frac{17Eh^3}{630(1+\nu)}\left(\frac{\partial^2\varphi_y}{\partial x^2}+\frac{\partial^2\varphi_x}{\partial x\partial y}\right)-\frac{8Gh}{15}\left(\varphi_y+\frac{\partial w}{\partial y}\right)=0. \tag{11c}$$

3 Non-local plate theories for axial buckling of SLGSs

3.1 Eringen's non-local elasticity

Eringen [59] introduced the non-local elasticity theory. For isotropic and homogenous elastic continuum, linear non-local elasticity theory is written as

$$\left(1-\mu\nabla^2\right)\sigma_{kl,l}(x)=\sigma_{kl}(x), \tag{12}$$

where μ non-local or small scale parameter depends on the material and internal characteristic constant and ∇ is the Laplacian operator. Also, the value of non-local parameter relied on the number of modes, the nature of motion, supporting conditions, the number of walls and layers, etc. There are only a few studies on the exact value of this parameter. Available data revealed that the acceptable range for non-local parameter was 0 to 4 nm^2 and, therefore, in this study this interval was used for this parameter.

3.2 Application of elastic foundation and non-local elasticity on plate theories

The SLGSs evaluated in this work were surrounded by elastic foundation. The elastic surrounding was simulated using Pasternak foundation model [25] (fig. 2). The loading of this foundation model was

$$Q_{pasternak}=k_w w-k_S\left(\frac{\partial^2 w}{\partial x^2}+\frac{\partial^2 w}{\partial y^2}\right), \tag{13}$$

where k_S is the Pasternak modulus parameter relevant to the in-plane shear stiffness of the medium and k_w is the Winkler modulus parameter. The foundation model was reduced to Winkler model by neglecting shear deformation effects ($k_S=0$) [24].

3.2.1 Classical plate theory (CLPT)

Based on the principle of virtual work, the governing differential equations for the aforementioned problem are derived [45]. By the adding elastic foundation terms to the governing equation of CLPT, we found

$$-\frac{Eh^3}{12(1-\nu^2)}\left(\frac{\partial^4 w}{\partial x^4}+2\nu\frac{\partial^4 w}{\partial x^2\partial y^2}+\frac{\partial^4 w}{\partial y^4}\right)-\frac{Eh^3}{6(1+\nu)}\frac{\partial^4 w}{\partial x^2\partial y^2}-P\frac{\partial^2 w}{\partial x^2}-K_w w+K_s\left(\frac{\partial^2 w}{\partial x^2}+\frac{\partial^2 w}{\partial y^2}\right)=0. \tag{14}$$

Based on eq. (12), there was only one constitutive relation for non-local CLPT model with elastic medium as

$$\begin{aligned}&-\frac{Eh^3}{12(1-\nu^2)}\left(\frac{\partial^4 w}{\partial x^4}+2\nu\frac{\partial^4 w}{\partial x^2\partial y^2}+\frac{\partial^4 w}{\partial y^4}\right)-\frac{Eh^3}{6(1+\nu)}\frac{\partial^4 w}{\partial x^2\partial y^2}-P\frac{\partial^2 w}{\partial x^2}+\mu P\left(\frac{\partial^4 w}{\partial x^4}+\frac{\partial^4 w}{\partial x^2\partial y^2}\right)-K_w w\\&+K_s\left(\frac{\partial^2 w}{\partial x^2}+\frac{\partial^2 w}{\partial y^2}\right)+\mu K_w\left(\frac{\partial^2 w}{\partial x^2}+\frac{\partial^2 w}{\partial y^2}\right)-K_s\left(\frac{\partial^4 w}{\partial x^4}+2\frac{\partial^4 w}{\partial x^2\partial y^2}+\frac{\partial^4 w}{\partial y^4}\right)=0.\end{aligned} \tag{15}$$

3.2.2 First-order shear deformation theory (FSDT)

Introduction of elastic foundation terms into governing equations of FSDT gives

$$\kappa Gh\left(\frac{\partial\varphi_x}{\partial x}+\frac{\partial\varphi_y}{\partial y}+\frac{\partial^2 w}{\partial x^2}+\frac{\partial^2 w}{\partial y^2}\right)-P\frac{\partial^2 w}{\partial x^2}-K_w w+K_s\left(\frac{\partial^2 w}{\partial x^2}+\frac{\partial^2 w}{\partial y^2}\right)=0, \tag{16a}$$

$$\frac{Eh^3}{12(1-\nu^2)}\left(\frac{\partial^2\varphi_x}{\partial x^2}+\nu\frac{\partial^2\varphi_y}{\partial x\partial y}\right)+\frac{Eh^3}{24(1+\nu)}\left(\frac{\partial^2\varphi_x}{\partial x\partial y}+\frac{\partial^2\varphi_y}{\partial y^2}\right)-\kappa Gh\left(\varphi_x+\frac{\partial w}{\partial x}\right)=0, \tag{16b}$$

$$\frac{Eh^3}{12(1-\nu^2)}\left(\frac{\partial^2\varphi_y}{\partial y^2}+\nu\frac{\partial^2\varphi_x}{\partial x\partial y}\right)+\frac{Eh^3}{24(1+\nu)}\left(\frac{\partial^2\varphi_x}{\partial x^2}+\frac{\partial^2\varphi_y}{\partial x\partial y}\right)-\kappa Gh\left(\varphi_y+\frac{\partial w}{\partial y}\right)=0. \tag{16c}$$

Based on eq. (13), non-local FSDT model constitutive relations with elastic foundation are

$$\begin{aligned}&\kappa Gh\left(\frac{\partial\varphi_x}{\partial x}+\frac{\partial\varphi_y}{\partial y}+\frac{\partial^2 w}{\partial x^2}+\frac{\partial^2 w}{\partial y^2}\right)-P\frac{\partial^2 w}{\partial x^2}+\mu P\left(\frac{\partial^4 w}{\partial x^4}+\frac{\partial^4 w}{\partial x^2\partial y^2}\right)-K_w w+K_s\left(\frac{\partial^2 w}{\partial x^2}+\frac{\partial^2 w}{\partial y^2}\right)\\&+\mu K_w\left(\frac{\partial^2 w}{\partial x^2}+\frac{\partial^2 w}{\partial y^2}\right)-K_s\left(\frac{\partial^4 w}{\partial x^4}+2\frac{\partial^4 w}{\partial x^2\partial y^2}+\frac{\partial^4 w}{\partial y^4}\right)=0,\end{aligned} \tag{17a}$$

$$\frac{Eh^3}{12(1-\nu^2)}\left(\frac{\partial^2\varphi_x}{\partial x^2}+\nu\frac{\partial^2\varphi_y}{\partial x\partial y}\right)+\frac{Eh^3}{24(1+\nu)}\left(\frac{\partial^2\varphi_y}{\partial x\partial y}+\frac{\partial^2\varphi_x}{\partial y^2}\right)-\kappa Gh\left(\varphi_x+\frac{\partial w}{\partial x}\right)=0, \tag{17b}$$

$$\frac{Eh^3}{12(1-\nu^2)}\left(\frac{\partial^2\varphi_y}{\partial y^2}+\nu\frac{\partial^2\varphi_x}{\partial x\partial y}\right)+\frac{Eh^3}{24(1+\nu)}\left(\frac{\partial^2\varphi_y}{\partial x^2}+\frac{\partial^2\varphi_x}{\partial x\partial y}\right)-\kappa Gh\left(\varphi_y+\frac{\partial w}{\partial y}\right)=0. \tag{17c}$$

3.2.3 Higher-order shear deformation theory (HSDT)

Introduction of elastic foundation terms into the governing equations of HSDT gives

$$\begin{aligned}&\frac{8Gh}{15}\left(\frac{\partial\varphi_x}{\partial x}+\frac{\partial\varphi_y}{\partial y}+\frac{\partial^2 w}{\partial x^2}+\frac{\partial^2 w}{\partial y^2}\right)+\frac{4Eh^3}{315(1-\nu^2)}\left[\frac{\partial^3\varphi_x}{\partial x^3}+\frac{\partial^3\varphi_y}{\partial y^3}+\nu\left(\frac{\partial^3\varphi_x}{\partial x\partial y^2}+\frac{\partial^3\varphi_y}{\partial x^2\partial y}\right)\right]-\frac{4Eh^3}{252(1-\nu^2)}\left(\frac{\partial^4 w}{\partial x^4}+\right.\\&\left.\frac{\partial^4 w}{\partial y^4}+2\nu\frac{\partial^4 w}{\partial x^2\partial y^2}\right)+\frac{4Eh^3}{315(1+\nu)}\left(\frac{\partial^3\varphi_x}{\partial x^2\partial y}+\frac{\partial^3\varphi_y}{\partial x\partial y^2}\right)-\frac{Eh^3}{126(1+\nu)}\frac{\partial^4 w}{\partial x^2\partial y^2}-P\frac{\partial^2 w}{\partial x^2}-K_w w+K_s\left(\frac{\partial^2 w}{\partial x^2}+\frac{\partial^2 w}{\partial y^2}\right)=0,\end{aligned} \tag{18a}$$

$$\begin{aligned}&\frac{17Eh^3}{315(1-\nu^2)}\left(\frac{\partial^2\varphi_x}{\partial x^2}+\nu\frac{\partial^2\varphi_y}{\partial x\partial y}\right)-\frac{4Eh^3}{315(1-\nu^2)}\left(\frac{\partial^3 w}{\partial x^3}+\nu\frac{\partial^3 w}{\partial x\partial y^2}\right)+\frac{17Eh^3}{630(1+\nu)}\left(\frac{\partial^2\varphi_x}{\partial x\partial y}+\frac{\partial^2\varphi_y}{\partial y^2}\right)\\&-\frac{4Eh^3}{315(1+\nu)}\frac{\partial^3 w}{\partial x\partial y^2}-\frac{8Gh}{15}\left(\varphi_x+\frac{\partial w}{\partial x}\right)=0,\end{aligned} \tag{18b}$$

$$\begin{aligned}&\frac{17Eh^3}{315(1-\nu^2)}\left(\frac{\partial^2\varphi_y}{\partial y^2}+\nu\frac{\partial^2\varphi_x}{\partial x\partial y}\right)-\frac{4Eh^3}{315(1-\nu^2)}\left(\frac{\partial^3 w}{\partial y^3}+\nu\frac{\partial^3 w}{\partial x^2\partial y}\right)+\frac{17Eh^3}{630(1+\nu)}\left(\frac{\partial^2\varphi_x}{\partial x^2}+\frac{\partial^2\varphi_y}{\partial x\partial y}\right)\\&-\frac{4Eh^3}{315(1+\nu)}\frac{\partial^3 w}{\partial x^2\partial y}-\frac{8Gh}{15}\left(\varphi_y+\frac{\partial w}{\partial y}\right)=0.\end{aligned} \tag{18c}$$

Based on eq. (13), constitutive relations for non-local HSDT model with elastic foundation are

$$\frac{8Gh}{15}\left(\frac{\partial\varphi_x}{\partial x}+\frac{\partial\varphi_y}{\partial y}+\frac{\partial^2 w}{\partial x^2}+\frac{\partial^2 w}{\partial y^2}\right)+\frac{4Eh^3}{315(1-\nu^2)}\left[\frac{\partial^3\varphi_x}{\partial x^3}+\frac{\partial^3\varphi_y}{\partial y^3}+\nu\left(\frac{\partial^3\varphi_x}{\partial x\partial y^2}+\frac{\partial^3\varphi_y}{\partial x^2\partial y}\right)\right]$$
$$-\frac{4Eh^3}{252(1-\nu^2)}\left(\frac{\partial^4 w}{\partial x^4}+\frac{\partial^4 w}{\partial y^4}+2\nu\frac{\partial^4 w}{\partial x^2\partial y^2}\right)$$
$$+\frac{4Eh^3}{315(1+\nu)}\left(\frac{\partial^3\varphi_y}{\partial x^2\partial y}+\frac{\partial^3\varphi_x}{\partial x\partial y^2}\right)-\frac{Eh^3}{126(1+\nu)}\frac{\partial^4 w}{\partial x^2\partial y^2}-k_w w$$
$$+\mu k_w\left(\frac{\partial^2 w}{\partial x^2}+\frac{\partial^2 w}{\partial y^2}\right)-\mu k_S\left(\frac{\partial^4 w}{\partial x^4}+2\frac{\partial^4 w}{\partial x^2\partial y^2}+\frac{\partial^4 w}{\partial y^4}\right)=0, \tag{19a}$$

$$\frac{17Eh^3}{315(1-\nu^2)}\left(\frac{\partial^2\varphi_x}{\partial x^2}+\nu\frac{\partial^2\varphi_y}{\partial x\partial y}\right)-\frac{4Eh^3}{315(1-\nu^2)}\left(\frac{\partial^3 w}{\partial x^3}+\nu\frac{\partial^3 w}{\partial x\partial y^2}\right)$$
$$+\frac{17Eh^3}{630(1+\nu)}\left(\frac{\partial^2\varphi_y}{\partial x\partial y}+\frac{\partial^2\varphi_x}{\partial y^2}\right)-\frac{4Eh^3}{315(1+\nu)}\frac{\partial^3 w}{\partial x\partial y^2}=0, \tag{19b}$$

$$\frac{17Eh^3}{315(1-\nu^2)}\left(\frac{\partial^2\varphi_y}{\partial y^2}+\nu\frac{\partial^2\varphi_x}{\partial x\partial y}\right)-\frac{4Eh^3}{315(1-\nu^2)}\left(\frac{\partial^3 w}{\partial y^3}+\nu\frac{\partial^3 w}{\partial y\partial x^2}\right)$$
$$+\frac{17Eh^3}{630(1+\nu)}\left(\frac{\partial^2\varphi_y}{\partial x^2}+\frac{\partial^2\varphi_x}{\partial x\partial y}\right)-\frac{4Eh^3}{315(1+\nu)}\frac{\partial^3 w}{\partial y\partial x^2}=0. \tag{19c}$$

4 Analytical solution for simply supported SLGSs

4.1 Analytical solutions for critical axial buckling load

Analytical solutions were obtained to provide critical axial buckling loads for all non-local theories for SLGSs in elastic foundation [45]. Simply supported boundary conditions were expressed as follows.

At $x=0$ and $x=L$:

$$w=0, \qquad \varphi_y=0, \qquad M_{xx}=0. \tag{20a}$$

At $y=0$ and $y=L$:

$$w=0, \qquad \varphi_x=0, \qquad M_{yy}=0. \tag{20b}$$

To satisfy boundary conditions, transverse and angular displacements were assumed to be in the following general form:

$$w(x,y)=\sum_{m=1}^{\infty}\sum_{n=1}^{\infty}W_{mn}\sin\left(\frac{m\pi x}{L}\right)\sin\left(\frac{n\pi y}{L}\right), \tag{21a}$$

$$\varphi_x(x,y)=\sum_{m=1}^{\infty}\sum_{n=1}^{\infty}A_{mn}\cos\left(\frac{m\pi x}{L}\right)\sin\left(\frac{n\pi y}{L}\right), \tag{21b}$$

$$\varphi_y(x,y)=\sum_{m=1}^{\infty}\sum_{n=1}^{\infty}B_{mn}\sin\left(\frac{m\pi x}{L}\right)\cos\left(\frac{n\pi y}{L}\right). \tag{21c}$$

By substituting eq. (21) into the equations of all non-local plate theories and solving them, critical axial buckling loads of SLGSs embedded in elastic foundation were obtained as follows.

For CLPT:

$$P_{CLPT}=\left(-3K_wL^4\nu^4-6\mu K_wm^2\pi^2L^2\nu^2-12\mu K_sm^4\pi^4\nu^2-8K_sm^2\pi^2L^2\nu^2+Eh^3m^4\pi^4\right.$$
$$\left.+6K_sm^2\pi^2L^2+3K_wL^4+14\mu K_sm^4\pi^4+6\mu K_wm^2\pi^2L^2\right)/\left(3m^2\pi^2\left(2m^2\pi^2\mu\nu^2+L^2\nu^2-L^2-2m^2\pi^2\mu\right)\right). \tag{22}$$

For FSDT:

$$P_{FSDT}=\left(-4E\mu K_sm^6\pi^6h^2-2Em^4\pi^4\kappa GL^2h^3-2Em^4\pi^4K_sL^2h^2-2Em^4\pi^4\mu K_wL^2h^2\right.$$
$$-Em^2\pi^2K_wL^4h^2-24m^4\pi^4\mu K_s\kappa GL^2+22m^4\pi^4\mu K_s\kappa GL^2\nu^2-12m^2\pi^2\mu K_w\kappa GL^4$$
$$\left.+12m^2\pi^2K_s\kappa GL^4\nu^2-12m^2\pi^2K_s\kappa GL^4+12m^2\pi^2\mu K_w\kappa GL^4\nu^2-6K_wL^6\kappa G+6K_wL^6\kappa G\nu^2\right)/$$
$$\left(m^2\pi^2\left(2E\mu m^4\pi^4h^2+Em^2\pi^2L^2h^2+12m^2\pi^2\mu\kappa GL^2-12m^2\pi^2\mu\kappa GL^2\nu^2+6\kappa GL^4-8\kappa GL^4\nu^2\right)\right). \tag{23}$$

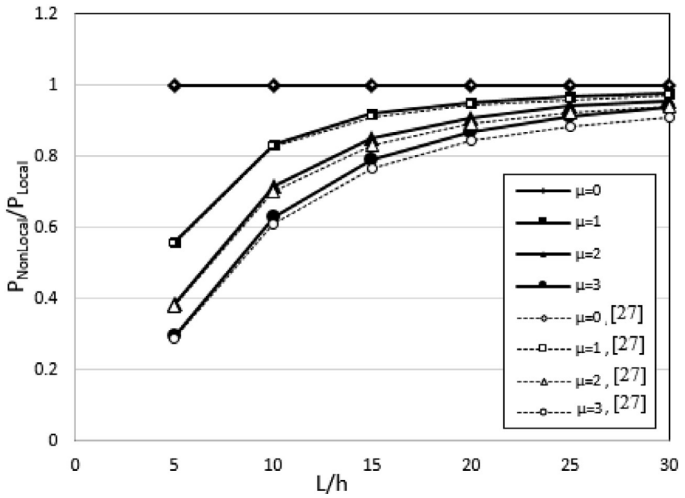

Fig. 3. Comparison and validation of the proposed model with Pradhan *et al.* model [27].

For HSDT:

$$\begin{aligned}P_{HSDT} = {} & \left(m^6\pi^6E^2h^5 - 1020Em^6\pi^6\mu K_sh^2\nu^2 + 1020Em^6\pi^6\mu K_sh^2 - 420Em^4\pi^4GL^2h^3\nu^2\right.\\ & + 420Em^4\pi^4GL^2h^3 - 510Em^4\pi^4\mu K_wL^2h^2\nu^2 + 510Em^4\pi^4K_sL^2h^2 + 510Em^4\pi^4\mu K_wL^2h^2\\ & - 510Em^4\pi^4K_sL^2h^2\nu^2 - 255Em^2\pi^2K_wL^4h^2\nu^2 + 255Em^2\pi^2K_wL^4h^2 + 5040m^4\pi^4\mu K_sGL^2\nu^4\\ & - 10080m^4\pi^4\mu K_sGL^2\nu^2 + 5040m^4\pi^4\mu K_sGL^2 + 2520m^2\pi^2\mu K_wGL^4 + 2520m^2\pi^2\mu K_wGL^4\nu^4\\ & + 2520m^2\pi^2K_sGL^4\nu^4 - 5040m^2\pi^2K_sGL^4\nu^2 + 2520m^2\pi^2K_sGL^4 - 5040m^2\pi^2\mu K_wGL^4\nu^2\\ & +1260K_wGL^6\nu^4 - 2520K_wGL^6\nu^2 + 1260K_wGL^6\big) / \big(17m^2\pi^2\left(34E\mu m^4\pi^4h^2\nu^2\right.\\ & - 34E\mu m^4\pi^4h^2 + 17Em^2\pi^2L^2h^2\nu^2 - 17Em^2\pi^2L^2h^2 - 168m^2\pi^2\mu GL^2\nu^4\\ & \left.\left.+336m^2\pi^2\mu GL^2\nu^2 - 168m^2\pi^2\mu GL^2 - 84GL^4 + 168GL^4\nu^2 - 84GL^4\nu^2\right)\right)\end{aligned} \tag{24}$$

It must be kept in mind that in the above explicit equations, it was assumed that $m = n$.

5 Results and discussion

The following properties were assumed for SLGSs for validation: $E = 1\,\text{TPa}$, $\nu = 0.16$, $h = 0.34\,\text{nm}$ and the side length (L) of the square SLGSs ranged between $\frac{L}{h} = 10$ and 40 [27]. As is shown in fig. 3, these findings were compared with the results obtained by Pradhan *et al.* [27] for buckling. When the elastic parameters are equal to zero, this means that the foundation is removed and there should not be any difference between the results of the present paper with Pradhan's paper. As can be seen in fig. 3, the results perfectly matched.

The comparison of the load ratios for different non-local plate theories with different non-local parameters are shown in fig. 3. It was seen that the effect of non-locality was more important in FSDT compared to other theories. These differences were higher when the value of non-local parameter was in the range of 0.25 to $1.75\,\text{nm}^2$.

Regarding elastic foundation, axial buckling load was enhanced for all non-local parameter values, which was more important at higher aspect ratios for all non-local parameter values and mode numbers. According to fig. 4, the stiffness of SLGSs was increased by enhancing Winkler modulus parameter, which was more important for lower buckling mode numbers.

Figures 5–8 show the effects of different parameters on critical axial buckling load. Note that HSDT theory is used for these curves. The effect of Winkler modulus parameter on the axial buckling loads of SLGSs for different mode numbers are shown in fig. 5. For the third mode, the increase of Winkler modulus is almost ineffective and critical buckling load is almost constant with increasing Winkler modulus.

The effect of Winkler modulus on the axial buckling loads of SLGSs for different aspect ratios in the range of $\mu = 1$ to $4\,\text{nm}^2$ are shown in fig. 6. Surrounding elastic was simulated using Winkler foundation model ($k_s = 0$) and it was found that the effect of k_w was enhanced for higher aspect ratios. The effect of the Winkler modulus on the axial buckling loads of SLGSs with different non-local values is shown in fig. 7. It was considered that $L/h = 10$ and 30. Similar to previous example, the Winkler foundation model ($k_s = 0$) was applied to the simulation of surrounding

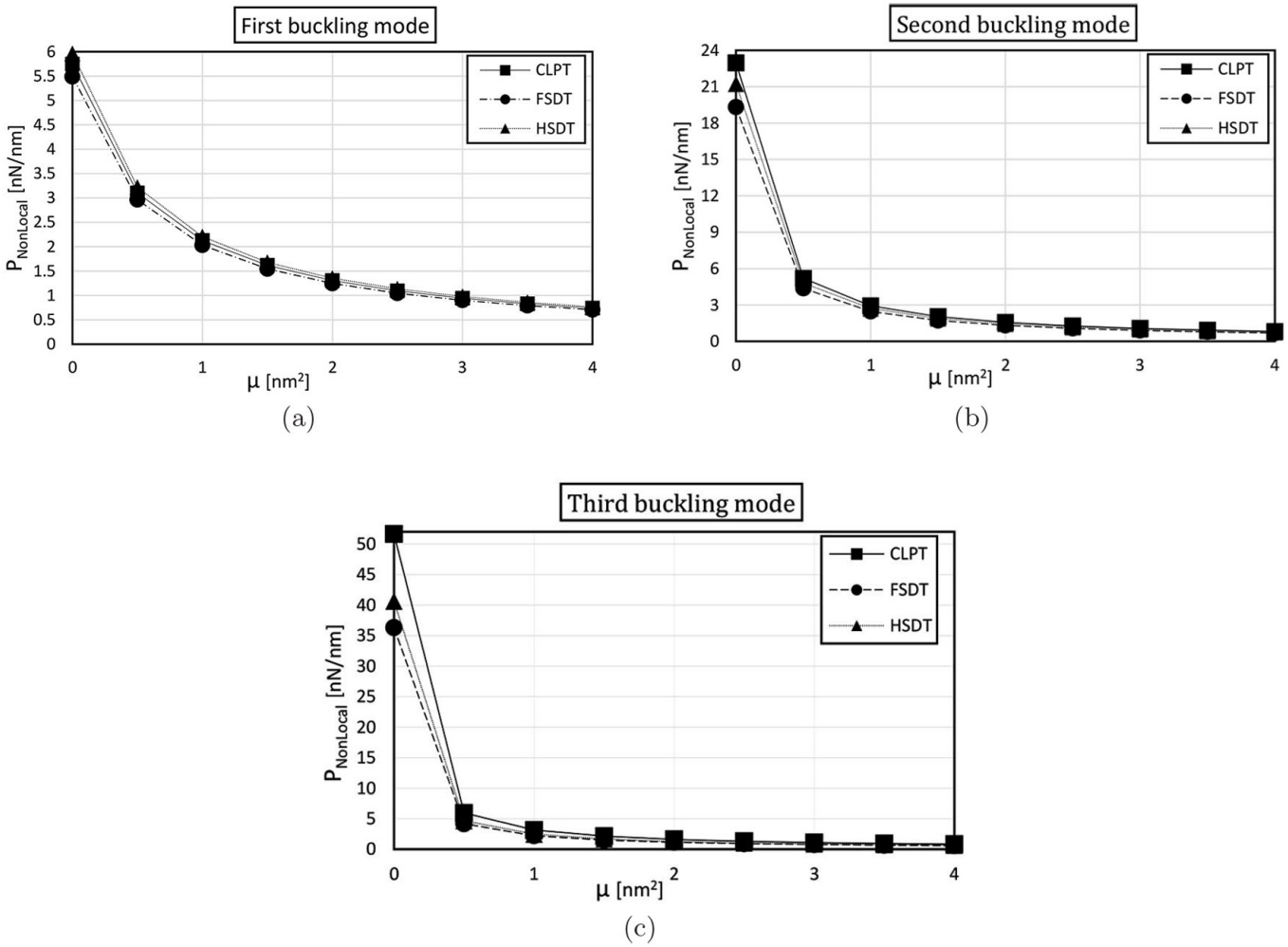

Fig. 4. The values of load ratio for different non-local plate theories: (a) first buckling mode; (b) second buckling mode; (c) third buckling mode.

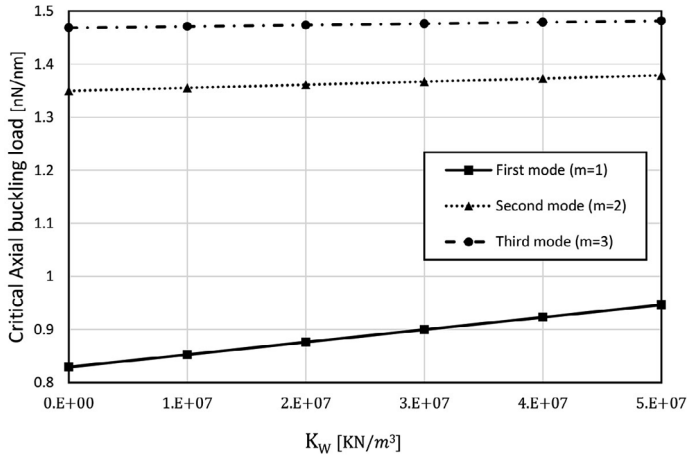

Fig. 5. Axial buckling loads with Winkler modulus parameter for different mode numbers ($\mu = 2\,\mathrm{nm}^2$, $L/h = 20$).

elastic medium. Surrounding elastic medium was considered as Pasternak foundation model with $k_w = 10^7\,\mathrm{KN/m}^3$. This effect for $L/h = 10$ and $L/h = 40$, are shown in figs. 8(a) and (b), respectively. It was seen that higher aspect ratios of SLGSs, enhanced the effect of k_s on critical axial buckling load but as mentioned earlier, the effect of non-locality was decreased at higher aspect ratios.

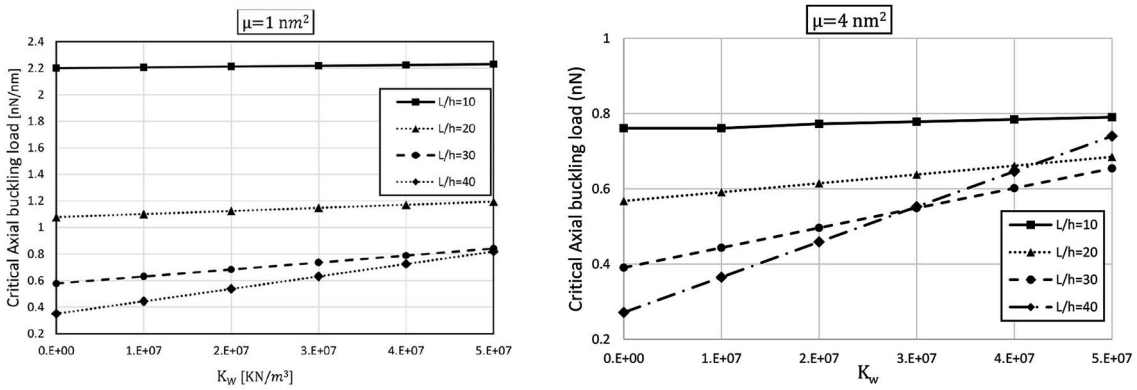

(a) (b)

Fig. 6. Axial buckling load for different Winkler modulus and aspect ratios: (a) $\mu = 1\,\mathrm{nm}^2$; (b) $\mu = 4\,\mathrm{nm}^2$.

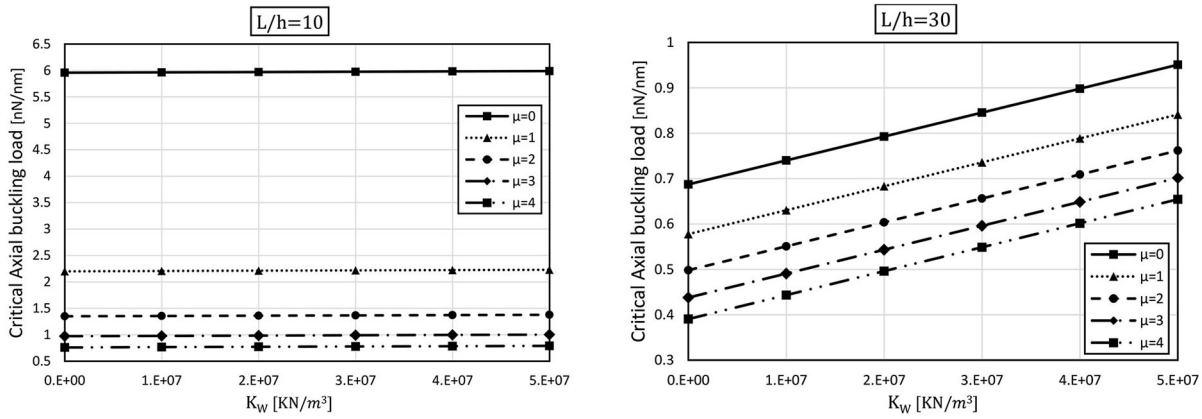

(a) (b)

Fig. 7. Axial buckling loads with the Winkler modulus for different values of non-local parameter: (a) $L/h = 10$; (b) $L/h = 30$.

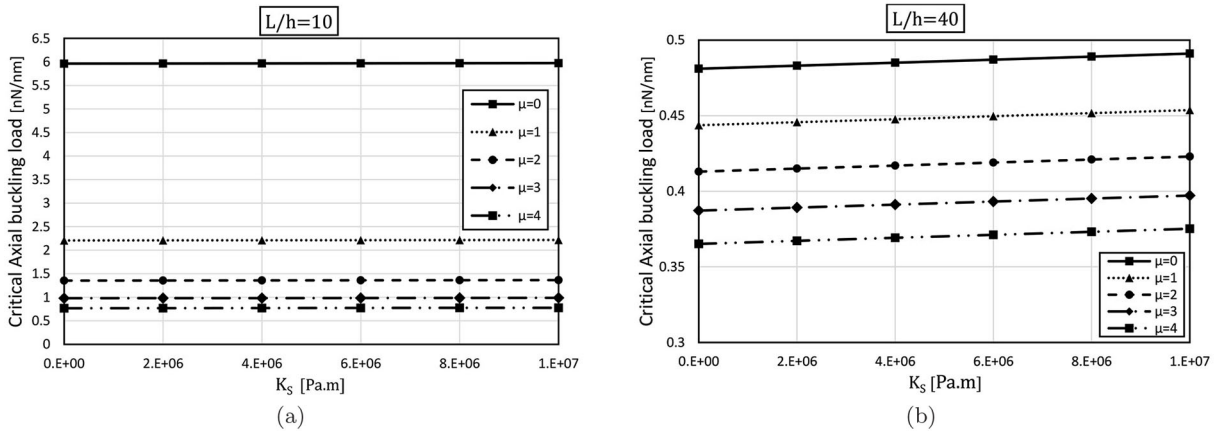

(a) (b)

Fig. 8. Axial buckling loads with the Pasternak modulus for different values of non-local parameter: (a) $L/h = 10$; (b) $L/h = 40$.

The variation of $\Omega = \frac{p_{with\ elastic\ foundation}}{p_{without\ elastic\ foundation}}$ for SLGSs obtained from different elastic foundation models with different aspect ratios are shown in fig. 9(a). The same results for different values of non-local parameter are plotted in fig. 9(b). It was considered that for the Winkler foundation model $k_w = 10^7\,\mathrm{KN/m^3}$ and for the Pasternak foundation model $k_w = 10^7 10^7\,\mathrm{KN/m^3}$, $k_s = 2 \times 10^6 10^7\,\mathrm{Pa \cdot m}$. It was seen that higher values of non-local parameter and aspect ratio, enhanced the differences between critical axial buckling loads predicted by Winkler and Pasternak foundation models. Also, it was observed that all non-local plate theories had almost similar patterns especially in aspect ratio variation.

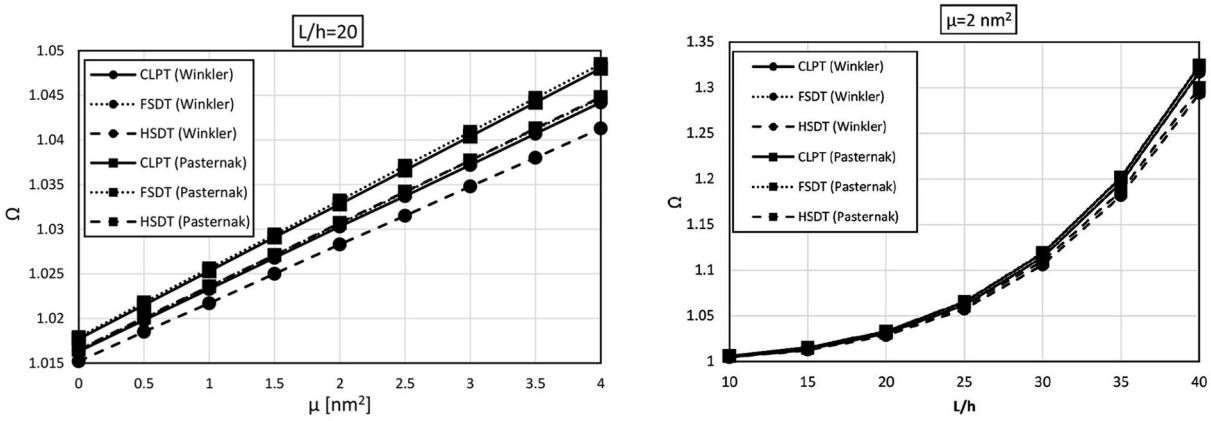

(a) (b)

Fig. 9. Comparison of the values of $\frac{P_{with\ elastic\ foundation}}{P_{without\ elastic\ foundation}}$ obtained from Winkler and Pasternak foundation models with different (a) non-local parameters ($L/h = 20$) and (b) aspect ratios ($\mu = 2\,\mathrm{mn}^2$).

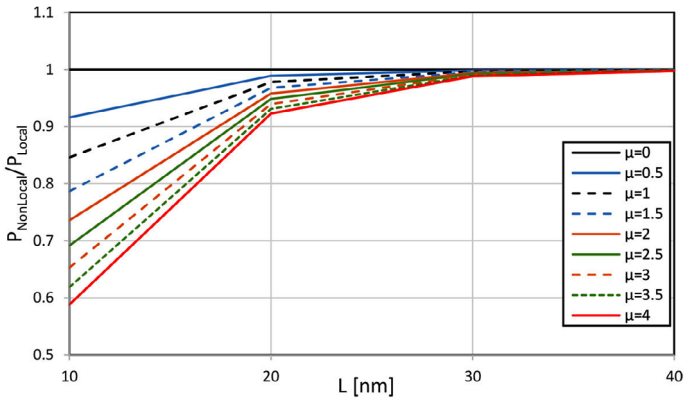

Fig. 10. Changes of buckling load along with the effectiveness of length and non-local parameter.

6 The effect of non-local parameter considering length only

Figure 10 shows more comprehensive investigation of the effect of non-local parameter when only the effect of length on the buckling behavior of the sheet was evaluated. By increasing the value of non-local parameter, the ratio of non-local load to local load was decreased. This trend was changed in lower lengths.

However, it was observed that by increasing the values of both non-local parameter and aspect ratio, the difference between critical axial buckling load obtained from Winkler and Pasternak models were also increased. Also, it was seen that there were almost similar patterns for this increase. The moduli of Winkler and Pasternak affected buckling behavior and increased buckling load in both theories. This change followed an almost similar trend in all three classical, first order shear, and higher order shear theories.

Based on the findings of this study, it was concluded that due to elastic medium, increase of axial buckling load occurred at all values of non-local parameter and this increase was more significant for higher aspect ratios in all modes and attracted more attention.

It was also revealed that critical axial loading on single-layer graphene sheets simulated by Pasternak model was almost similar to all non-layered sheet theories, especially regarding variation of aspect ratio. In addition, higher differences were observed for higher aspect ratios and non-local parameters. The most important conclusions are presented below:

- The effects of small scale on the buckling behavior of graphene nano-sheets on elastic substrate were significant.
- Increasing the value of Winkler and Pasternak parameters increased critical buckling loads on graphene nano-sheets in elastic medium.
- Elastic foundation with appropriate Winkler coefficient can increase critical buckling force.
- Increase of Pasternak shear coefficient in elastic medium also increased the stiffness of the structure.

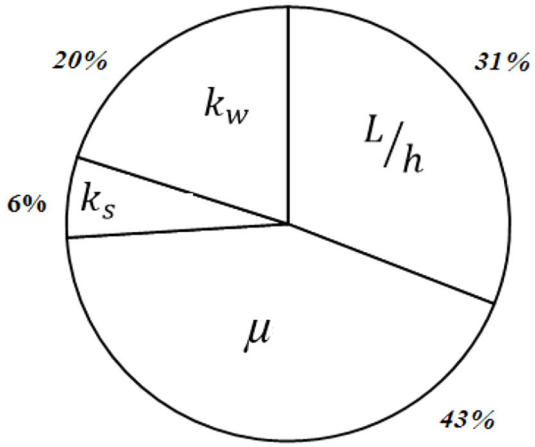

Fig. 11. Sensitivity of effective parameters on PHSDT.

7 Global sensitivity analysis

The aim of global sensitivity analysis (GSA) is to investigate the effect of changes of input parameters on model outputs. In this way, the roles of different input parameters in the distribution domain of inputs can be identified and the average effect of inputs on outputs can be comprehensively considered. GSA can determine the significance sequence of model inputs as well. One kind of GSA is variance-based Sobol method [61]. This kind of methods decompose output variances into separate parts which could be assigned to different input variables and their interactions.

In this work, Sobol-based GSA was used to PHSDT as output by coding in MATLAB. Figure 11 shows total effective parameters and Sobol indices. The obtained results demonstrated that the most significant factor was μ; but the effects of k_w and L/h were also important.

8 Conclusion

In this study, axial buckling behaviors of SLGSs surrounded by elastic foundation have been investigated. Pasternak and Winkler foundation models were applied to simulate a surrounding elastic medium. Analytical solutions were achieved for SLGSs with simply supported boundary conditions to consider the effect of small scale on buckling. Explicit relations were achieved for calculating the axial buckling loads of SLGSs with different non-local plate theories.

In this work, we revealed that by considering elastic foundations, axial buckling loads increased for all non-local parameter values and this increase was more important at high aspect ratios. Moreover, it was shown that, non-locality had the strongest effect in FSDT, especially for a certain range of non-local parameter, among different types of non-local plate theories.

It was also shown that critical axial buckling loads of embedded SLGSs obtained from the pasternak foundation model was relatively higher compared to those simulated by the Winkler foundation model and this difference was almost similar in all non-local plate theories, especially in terms of the changing of aspect ratio. Furthermore, the difference was more significant at higher values of aspect ratio and non-local parameter.

Sobol-based GSA was employed to PHSDT as output by coding in MATLAB software. In addition, results demonstrated that the most significant factor was non-local parameter.

References

1. S. Kitipornchai, X.Q. He, K.M. Liew, Phys. Rev. B **72**, 075443 (2005).
2. K.M. Liew, X.Q. He, S. Kitipornchai, Acta Mater. **54**, 4229 (2006).
3. K. Behfar, R. Naghdabadi, Compos. Sci. Technol. **65**, 1159 (2005).
4. Z. Huang, Z. Qin, F. Chu, Compos. Struct. **153**, 96 (2016).
5. Z. Huang, Z. Qin, F. Chu, J. Sandw. Struct. Mater. **18**, 531 (2016).
6. Z. Huang, Z. Qin, F. Chu, J. Vib. Control **22**, 1876 (2016).

7. J. Peddieson, G.R. Buchanan, R.P. McNitt, Int. J. Eng. Sci. **41**, 305 (2003).
8. S. Sahmani, A.M. Fattahi, Mater. Res. Express **4**, 1 (2017).
9. H.S. Shen, J. Theor. Biol. **264**, 386 (2010).
10. S. Sahmani, A.M. Fattahi, Comput. Method Appl. Mech. Eng. **322**, 187 (2017).
11. S. Filiz, M. Aydogdu, Comput. Mater. Sci. **49**, 619 (2010).
12. L. Shen, H.S. Shen, C.L. Zhang, Comput. Mater. Sci. **48**, 680 (2010).
13. B. Safaei, A.M. Fattahi, Mechanics **23**, 678 (2017).
14. J. Yang, L.L. Ke, S. Kitipornchai, Physica E **42**, 1727 (2010).
15. M.J. Hao, X.M. Guo, Q. Wang, Eur. J. Mech. A/Solids **29**, 49 (2010).
16. M. Alizadeh, A.M. Fattahi, Eng. Comput. **35**, 215 (2018).
17. K. Kiani, Int. J. Mech. Sci. **52**, 1343 (2010).
18. A.M. Zenkour, Eur. Phys. J. Plus **133**, 193 (2018).
19. S. Sahmani, A.M. Fattahi, J. Mol. Graph Modell. **75**, 20 (2017).
20. A.M. Fattahi, S. Sahmani, Microsyst. Technol. **23**, 5121 (2017).
21. M.F. Chen, G.Y. Jin, Y.T. Zhang, F.L. Niu, Z.G. Liu, Compos. Struct. **207**, 304 (2019).
22. Y.K. Chen, G.Y. Jin, C.Y. Zhang, T.G. Ye, Y.Q. Xue, Compos. Part B Eng. **153**, 376 (2018).
23. A.M. Fattahi, S. Sahmani, Arab. J. Sci. Eng. **42**, 4617 (2017).
24. E. Winkler, *Theory of Elasticity and Strength* (H. Dominicus, Prague, 1867).
25. P.L. Pasternak, *On a new method of analysis of an elastic foundation by means of two foundation constants*, in *Gosudarstvennoe Izdatelstro Liberaturi po Stroitelstvui Arkhitekture* (Moscow, Russia, 1954).
26. K.M. Liew, X.Q. He, S. Kitipornchai, Acta Mater. **54**, 4229 (2006).
27. S.C. Pradhan, T. Murmu, Physica E **42**, 1293 (2010).
28. S. Azizi, B. Safaei, A.M. Fattahi, M. Tekere, Adv. Mater. Sci. Eng. **2015**, 318539 (2015).
29. R. Moradi-Dastjerdi, G. Payganeh, M. Tajdari, Polym. Compos. **38**, E542 (2017).
30. R. Moradi-Dastjerdi, G. Payganeh, M. Tajdari, Polym. Compos. **39**, 2190 (2018).
31. Z. Qin, X. Pang, B. Safaei, F. Chu, Compos. Struct. **220**, 847 (2019).
32. R. Moradi-Dastjerdi, H. Malek-Mohammadi, H. Momeni-Khabisi, Z. Angew. Math. Mech. **97**, 1418 (2017).
33. Z. Qin, Z. Yang, J. Zu, F. Chu, Int. J. Mech. Sci. **142-143**, 127 (2018).
34. Z. Qin, F. Chu, Z. Jean, Int. J. Mech. Sci. **133**, 91 (2017).
35. R. Shokri-Oojghaz, R. Moradi-Dastjerdi, H. Mohammadi, K. Behdinan, Polym. Compos. **40**, E1918 (2019).
36. B. Safaei, R. Moradi-Dastjerdi, F. Chu, Compos. Struct. **192**, 28 (2018).
37. B. Safaei, R. Moradi-Dastjerdi, Z. Qin, F. Chu, Compos. Part B Eng. **161**, 44 (2019).
38. B. Safaei, R. Moradi-Dastjerdi, Z. Qin, K. Behdina, F. Chu, J. Sandw. Struct. Mater. (2019) https://doi.org/10.1177/1099636219848282.
39. A. Bouadi, Anis, A.A. Bousahla, M.S.A. Houari, H. Heireche, A. Tounsi, Adv. Nano Res. **6**, 147 (2018).
40. F. Ebrahimi, M.R. Barati, Struct. Eng. Mech. **67**, 143 (2018).
41. T.H. Daouadji, B. Adim, Struct. Eng. Mech. **61**, 49 (2017).
42. M. Malikan, J. Appl. Comput. Mech. **4**, 1 (2018).
43. M. Malikan, Appl. Math. Model. **48**, 196 (2017).
44. B. Safaei, P. Naseradinmousavi, A. Rahmani, J. Mol. Graph Modell. **65**, 43 (2016).
45. A.M. Fattahi, B. Safaei, Microsyst. Technol. **23**, 5079 (2017).
46. M. Malikan, M. Jabbarzadeh, S. Dastjerdi, Microsyst. Technol. **23**, 2973 (2017).
47. M.E. Golmakani, M. Malikan, M.N. Sadraee Far, H.R. Majidi, Mater. Res. Express **5**, 065010 (2018).
48. M. Malikan, V.B. Nguyen, F. Tornabene, Eng. Sci. Technol. **21**, 778 (2018).
49. Y.Q. Xue, G.Y. Jin, H. Ding, M.F. Chen, Compos. Struct. **192**, 193 (2018).
50. Q. Wang, D. Shi, Q. Liang, X. Shi, Compos. Part B Eng. **88**, 264 (2016).
51. T. Liu, G. Hu, A. Wang, Q. Wang, Appl. Acoust. **155**, 407 (2019).
52. M. Malikan, J. Appl. Comput. Mech. **5**, 103 (2019).
53. M.E. Golmakani, M.N. Sadraee Far, Microsyst. Technol. **23**, 2145 (2017).
54. B. Safaei, N.A. Ahmed, A.M. Fattahi, Eur. Phys. J. Plus **134**, 271 (2019).
55. B. Safaei, A.M. Fattahi, F. Chu, Microsyst. Technol. **24**, 2663 (2018).
56. S. Azizi, A.M. Fattahi, J.T. Kahnamouei, Comput. Theor. Nanosc. **12**, 4179 (2015).
57. S. Roozpeikar, A.M. Fattahi, SN Appl. Sci. **1**, 17 (2018).
58. B. Safaei, Farzad Hamed Khoda, A.M. Fattahi, Adv. Nano Res. **7**, 267 (2019).
59. B. Safaei, R. Moradi-Dastjerdi, K. Behdinan, F. Chu, Aerospace Sci. Technol. **91**, 175 (2019).
60. A.C. Eringen, Int. J. Eng. Sci. **10**, 425 (1972).
61. I.M. Sobol, Math. Comput. Simul. **55**, 271 (2001).
62. G. Kirchhoff, Mathematik **40**, 51 (1850).
63. J.N. Reddy, J. Appl. Mech. **51**, 745 (1984).